Synthesis and Magnetic Properties of Silica-Coated FePt Nanocrystals

Doh C. Lee, Frederic V. Mikulec, José M. Pelaez, Bonil Koo, and Brian A. Korgel*

Department of Chemical Engineering, Texas Materials Institute, and Center for Nano- and Molecular Science and Technology, The University of Texas at Austin, Austin, Texas 78712-1062

Received: February 15, 2006; In Final Form: April 18, 2006

Colloidal FePt nanocrystals, 6 nm in diameter, were synthesized and then coated with silica (SiO_2) shells. The silica shell thickness could be varied from 10 to 25 nm. As-made FePt@SiO_2 nanocrystals have low magnetocrystalline anisotropy due to a compositionally disordered FePt core. When films of FePt@SiO_2 particles are annealed under hydrogen at 650 °C or above, the FePt core transforms to the compositionally ordered $L1_0$ phase, and superparamagnetic blocking temperatures exceeding room temperature are obtained. The SiO_2 shell prevents FePt coalescence at annealing temperatures up to ~850 °C. Annealing under air or nitrogen does not induce the FePt phase transition. The silica shell limits magnetic dipole coupling between the FePt nanocrystals; however, low temperature (5 K) and room temperature magnetization scans show slightly constricted hysteresis loops with coercivities that decrease systematically with decreased shell thickness, possibly resulting from differences in magnetic dipole coupling between particles.

Introduction

$L1_0$ FePt has high magnetocrystalline anisotropy (K_u), saturation magnetization, and maximum energy product $[BH]_{max}$ (6.6×10^7 erg/cm^3 (~60 meV/nm^3), 1140 emu/cm^3, and 13 MGOe, respectively), making it a good candidate material for high-density nonvolatile magnetic memory.[1−3] $L1_0$ FePt domains as small as 3 nm in diameter could be used as memory bits—their magnetic anisotropy energy (K_uV) would exceed kT (at room temperature) by about a factor of 25,[3,4] and 1 Tb/in.[2] storage density using 3 nm in diameter FePt domains as individual bits in a monolayer would require an edge-to-edge separation of about 25 nm. Pioneering work by Sun and Murray has led to a well-developed colloidal synthesis of FePt nanocrystals in this size range, and particles with narrow size distributions and good dispersion stability can be obtained. These colloidal nanocrystals, however, are compositionally disordered with very low magnetocrystalline anisotropy.[5,6] To obtain the $L1_0$ phase with high magnetocrystalline anisotropy, the nanocrystals must be cast into films and annealed at a relatively high temperature (>550 °C).[5] During annealing, the organic capping ligands decompose, and the particles sinter.[7,8] Sintering is a major problem that destroys the size distribution and leads to polycrystalline films.

Several approaches have been studied to alleviate the problem of sintering, including the addition of impurities such as Sb[9] or Cu[10] that lower the face-centered cubic (fcc) to $L1_0$ phase transition temperature, direct synthesis of the $L1_0$ phase using microwave radiation,[11] biomolecule-aided[12] particle growth, chemical tethering to substrates,[13] and the deposition of thermally resistant inorganic coatings. Although very interesting, the direct synthetic approaches to $L1_0$ FePt nanocrystals have thus far been relatively unsuccessful, with very low yields and poor magnetic properties. Substrate tethering is limited to nanocrystal monolayers, most likely not suitable for magnetic memory applications, as multilayers will be needed for sufficient detection signal. FePt nanocrystals have been embedded in a host matrix of carbon or hafnium oxide by gas-phase sputtering over a nanocrystal monolayer[14] or in salts such as NaCl by ball milling.[15] These host matrixes prevented sintering during annealing to the $L1_0$ phase. However, there is little control over the interparticle separation in the nanocrystal film or the coating thickness using these methods. Colloidal coating deposition methods can provide better control over the shell thickness of the protective layer. Iron oxide has been deposited as a shell material with good controlled coverage, with thicknesses of 2−5 nm.[16,17] Iron oxide is interesting because it will deposit as a shell during the nanocrystal synthesis simply by using a higher Fe concentration in the reaction mixture.[18] These iron oxide coatings have been shown to prevent FePt sintering up to ~700 °C, which is high enough for the fcc to $L1_0$ phase transition.[17] However, this approach adds a soft magnetic impurity to the FePt film, which Liu et al. showed to lead to very low coercivities relative to the sintered $L1_0$ FePt films obtained from the bare FePt particles.[17] A nonmagnetic thermally resistant coating that can be deposited with larger thicknesses is desired for many applications. Through the use of colloidal methods, silica shells have been deposited on ferrite,[19] iron oxide,[20−22] and recently FePt[23,24] nanocrystals. Yamamoto et al.[23] annealed their silica-coated FePt nanocrystals and found that FePt did not sinter at temperatures below 900 °C; however, an ability to tune silica shell thickness was not reported.

Here we demonstrate the encapsulation of 6 nm in diameter FePt nanocrystals in silica (SiO_2) shells (FePt@SiO_2) with tunable thicknesses from 10 to 25 nm. SiO_2 deposition was performed in water-in-oil microemulsions, and the SiO_2 layer thickness could be controlled simply by varying the ratio of the FePt nanocrystals to the silica precursor. The as-made FePt@SiO_2 nanocrystals disperse in polar solvents such as ethanol/water mixtures. Surface modification with octadecyltrimethoxysilane (OTMOS) yielded FePt@SiO_2 particles that were dispersible in nonpolar organic solvents. The silica shell prevents FePt sintering at annealing temperatures up to ~850 °C. Interestingly, annealing under nitrogen or air did not induce the fcc to $L1_0$ phase transition, even at temperatures as high as ~850

* Author to whom correspondence should be addressed. Phone: (512) 471-5633. Fax: (512) 471-7060. E-mail: korgel@che.utexas.edu.

10.1021/jp060974z CCC: $33.50
Published on Web 05/18/2006

°C. A hydrogen annealing environment was needed to induce the fcc to $L1_0$ phase transition at about 650 °C, which is higher in temperature compared to the organic-monolayer-coated nanocrystals (~550 °C). Field-cooled (FC) and zero-field-cooled (ZFC) temperature-dependent magnetization measurements showed that the 6 nm in diameter $L1_0$ nanocrystals exhibited a blocking temperature above room temperature. The coercivity depended on the silica shell thickness, increasing with increasing thickness, perhaps due to decreased magnetic dipole coupling between FePt domains.

Experimental Details

FePt Nanocrystals. FePt nanocrystals, 6 nm in diameter, were prepared by arrested precipitation using standard airless techniques on a Schlenk line according to methods reported by Chen et al.[18] Platinum acetylacetonate (0.5 mmol, $Pt(acac)_2$, 97%, Aldrich) was mixed with 10 mL of octyl ether (>97%, Fluka) in a 100 mL three-neck flask. The mixture was degassed for 1 h and then heated to 100 °C under N_2. Iron pentacarbonyl (1 mmol, $Fe(CO)_5$, Aldrich), 8 mmol of oleic acid (Aldrich), and 8 mmol of oleylamine (Fluka) were then injected while the mixture was stirred vigorously. The reaction mixture was heated at a rate of ~15 °C/min to 240 °C. The reaction mixture was then kept at 240 °C and stirred for 1 h. The reaction flask was then heated to reflux (295 °C) for 2 h. The reaction solution was cooled to room temperature by removing the heating source. The nanocrystals were then precipitated with excess ethanol and collected by centrifugation. The nanocrystals were redispersed in toluene and precipitated again with excess ethanol and collected by centrifugation.

Silica Coating Procedure. The FePt nanocrystals were coated with SiO_2 by base-catalyzed silica formation from tetraethylorthosilicate in a water-in-oil microemulsion.[19,22] Igepal CO-520 (8 mL, $(C_2H_4O)_n{\cdot}C_{15}H_{24}O$, $n \approx 5$, Aldrich) was mixed with 170 mL of cyclohexane (Aldrich) in a 250 mL Erlenmeyer flask and stirred. FePt nanocrystals were dispersed in cyclohexane at a concentration of 1 mg/mL and then injected into the cyclohexane/Igepal solution. The amount of FePt nanocrystals added ranged from 8 to 40 mg (i.e., 8 to 40 mL), depending on the desired silica shell thickness. Approximately 1.3 mL of 30% NH_4OH aqueous solution (EM Science) was then added dropwise and stirred for 2−3 min, followed by the addition of 1.5 mL of tetraethylorthosilicate (TEOS, 98%, Aldrich). Depending on the desired silica shell thickness, the amount of TEOS added was varied from 0.5 to 12 mL. Approximately 16 mL of FePt/cyclohexane dispersion with 1.5 mL of TEOS gave ~16-nm-thick SiO_2 shells. The mixture was stirred for 72 h before adding methanol to collect particles. The particles were precipitated with excess hexane and collected by centrifugation. The particles were redispersed in ethanol. The FePt@SiO_2 nanocrystals were "washed" using this procedure at least three times to remove excess surfactant. The final product was stored as an ethanol dispersion.

FePt@SiO_2 Annealing and OTMOS coating. The FePt@SiO_2 particles were annealed in a tube furnace (TF55035A, Lindberg/Blue M). The particles were drop-cast onto a Si wafer, positioned into a 1 in. in diameter quartz tube, and then placed in the tube furnace. Annealing was performed by purging the tube and the sample for 30 min with N_2 or 7% H_2/93% N_2 (purchased from Matheson Trigas) flow while heating at a rate of 60−70 °C/min. Samples annealed in air were not purged. The samples were annealed at the reported temperatures for 1 h.

Surface functionalization of the silica-coated nanoparticles was carried out using the method reported by Wang et al.[25] Approximately 10 mL of ethanol dispersion of FePt@SiO_2 particles at a concentration of 1 mg/mL was mixed with 0.1 mL of 30% NH_4OH aqueous solution. Approximately 0.5 mL of 10 vol % OTMOS (Aldrich) in $CHCl_3$ was added dropwise to the disperrsion, followed by stirring for 24 h.

Materials Characterization. The nanocrystals were characterized using transmission electron microscopy (TEM), energy dispersive X-ray spectroscopy (EDS), scanning electron microscopy (SEM), and X-ray diffraction (XRD).

TEM images were obtained using either a JEOL 2010F operated at an accelerating voltage of 200 kV or a Phillips EM208 transmission electron microscope at 80 kV. For TEM imaging, as-synthesized FePt nanocrystals were dispersed in chloroform and drop-cast on a carbon-coated 200-mesh Cu grid (Ladd Research). FePt@SiO_2 particles were similarly prepared for TEM imaging by dispersing the particles in ethanol and drop-casting onto a carbon-coated Cu TEM grid. Energy dispersive X-ray spectroscopy data were measured by an Oxford INCA EDS detector on the JEOL 2010F.

Scanning electron microscopy images were obtained on a LEO 1530 high-resolution scanning electron microscope operating between 1.5 and 3 kV with working distance between 2 and 6 mm. For SEM imaging, samples were prepared by dispersing in ethanol and then drop-casting onto a 2×2 cm^2 Si substrate (cut from 6 in. p-type (100) Si wafer, Nova Electronic Materials). The samples were not coated with metal.

X-ray diffraction was obtained on a quartz slide using a Bruker-Nonius D8 Advance diffractometer. Samples were typically scanned for ~12 h at a scan rate of 12 deg/min with 0.02 deg increments.

Magnetic properties were measured using a superconducting quantum interference device (SQUID, Quantum Design). The particles, either as-made or annealed, were collected in a gelatin capsule (Eli Lilly and Company) and inserted into the magnetometer. The temperature sweeps were collected under a constant field of 1 kOe from 5 to 300 K. The magnetization was also measured as a function of applied field at 5 and 300 K. The magnetization data presented in this paper are not background subtracted for the diamagnetic signal from the SiO_2 shell or the diamagnetic gelatin capsules because their contributions to the magnetic signal were negligible. At 50 kOe of applied field, the magnetization of the FePt@SiO_2 particles ranges from 1 to 10 emu/g while that of the pure SiO_2 particles ranges from 0.01 to 0.02 emu/g.

Results and Discussion

FePt@SiO_2 Nanocrystal Synthesis. Figure 1a shows a TEM image of the oleic acid/oleylamine-capped FePt nanocrystals that were coated with SiO_2. The nanocrystals were relatively size-monodisperse with an average diameter of 6 nm. EDS showed that the composition in the nanocrystal core was very close to 1:1 Fe/Pt, ranging statistically between 50:50 Fe/Pt and slightly Pt-rich particles, with a composition of 45:55. The particles do not appear to have a spherical morphology but rather a cuboidal shape. These FePt nanocrystals were coated with SiO_2 using nonionic surfactant-stabilized water-in-oil microemulsions as the reaction media. NH_4OH was used to catalyze the decomposition of TEOS to silica over the course of about 3 days.[26,27] Figures 1B and 1C show TEM images of a representative sample of SiO_2-coated FePt nanocrystals. These particles have 16.12 ± 1.81-nm-thick SiO_2 shells that were formed by mixing ~940 μL of TEOS with 10 mg of FePt nanocrytals. Each silica sphere encapsulates one FePt nano-

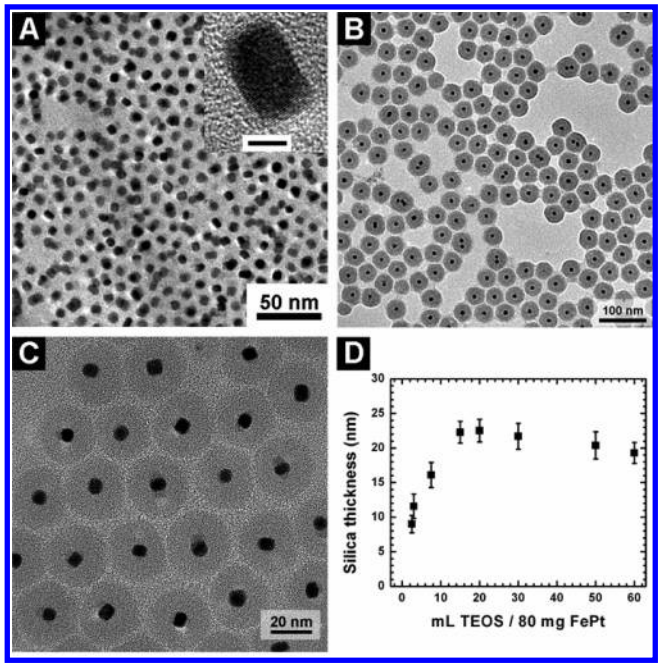

Figure 1. Transmission electron microscopy images of FePt nanocrystals (A) prior to and (B and C) after coating with SiO_2. (The inset scale bar in part A is 3 nm.) (D) The SiO_2 shell thickness obtained as a function of TEOS concentration.

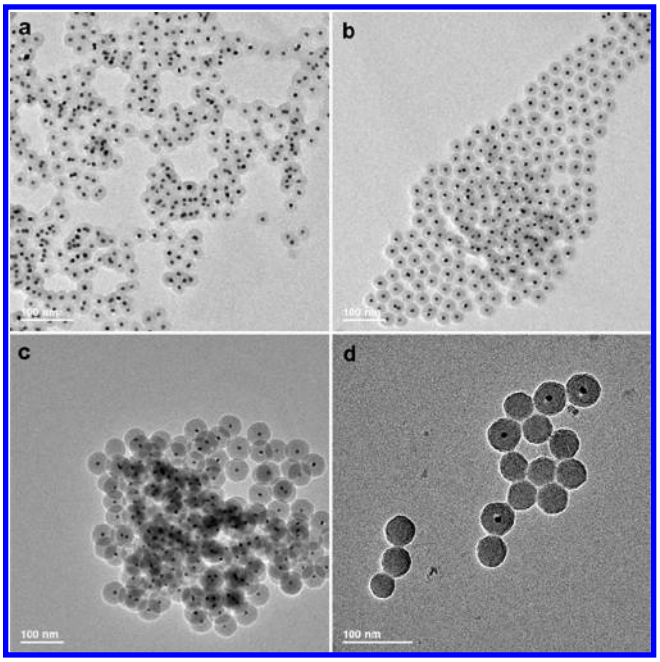

Figure 2. Transmission electron microscopy images of FePt@SiO_2 particles with different SiO_2 thicknesses. Samples were prepared by dispersing (a) 16 mg, (b) 40 mg, (c) 8 mg, or (d) 16 mg of FePt nanocrystals in 170 mL of cyclohexane and 8 mL of Igepal. Approximately 1.3 mL of 30% aqueous NH_4OH solution was added, followed by the addition of (a) 0.5 mL, (b) 1.5 mL, (c) 1.5 mL, or (d) 12 mL of TEOS. In part d, some of the silica particles do not have FePt nanocrystals at their core, which occurred more frequently at higher TEOS/FePt ratios. The SiO_2 thicknesses are (a) 9.02 ± 1.26 nm, (b) 11.59 ± 1.76 nm, (c) 23.28 ± 1.56 nm, and (d) 19.30 ± 1.52 nm. Figure 1d plots the measured silica shell thickness for several TEOS/FePt ratios.

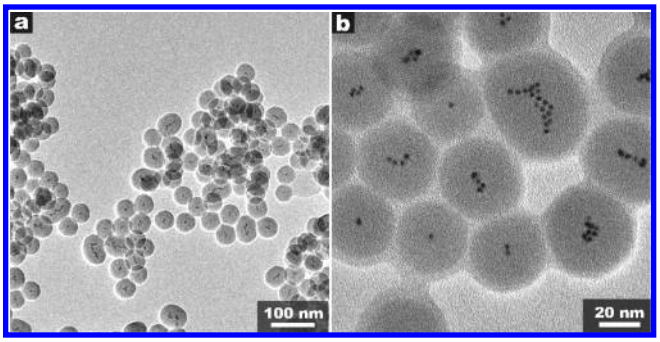

Figure 3. Transmission electron microscopy images of FePt@SiO_2 particles with multiple 2.7 nm in diameter FePt nanocrystals. A wide range of FePt concentrations and FePt/TEOS ratios were explored, yet reaction conditions could not be identified to encapsulate individually these smaller FePt nanocrystals in silica spheres.

crystal, although a small fraction of the silica particles has either two or zero FePt particles.

The SiO_2 shell thickness could be controlled from 7 to 23 nm by adjusting the TEOS concentration and the ratio of TEOS to FePt nanocrystals used during the coating step. Figure 1D plots the SiO_2 shell thickness obtained as a function of the TEOS/FePt ratio. Figure 2 shows TEM images of FePt@SiO_2 obtained with varying silica shell thickness. At low TEOS concentrations, increasing TEOS/FePt increased the shell thickness. Above TEOS/FePt ratios of ~15 mL TEOS/80 mg FePt, the shell thickness leveled off and decreased slightly with higher TEOS concentrations. In the range of higher TEOS concentrations, the silica sphere diameter plateaus, and more TEOS simply nucleates more FePt-free SiO_2 particles. As a result, the average shell thickness remains nearly constant at high TEOS concentrations, even when 3 times as much TEOS was used as in the case of Figure 1B.

When smaller 2.7 nm in diameter FePt nanocrystals were coated with silica, reaction conditions could not be identified to encapsulate individual nanocrystals. Regardless of the FePt concentration and the FePt/TEOS ratio, multiple FePt nanocrystals were encapsulated into the silica shells. Figure 3 shows TEM images of typical results.

Annealed FePt@SiO_2 Nanocrystals. The as-made FePt@SiO_2 nanocrystals are superparamagnetic at room temperature. Figure 4A shows FC and ZFC temperature sweeps of the magnetization under constant applied fields of 1000 Oe. The peak in the ZFC scan indicates that the as-made FePt@SiO_2 nanocrystals are superparamagnetic with a blocking temperature of ~30 K. This agrees with reported magnetic measurements on organic-coated as-made FePt nanocrystals.[28] Since the FePt diameter is 6 nm, the magnetocrystalline anisotropy is $\sim 2.3 \times 10^{-3}$ meV/nm^3, which is about 4 orders of magnitude lower than the bulk value for $L1_0$ FePt (~60 meV/ nm^3). At 5 K, which is below the blocking temperature, a field sweep shows hysteresis with a coercivity of ~2500 Oe (Figure 4A, inset).

To obtain the hard magnetic $L1_0$ FePt phase, the FePt@SiO_2 nanocrystals were drop-cast onto a silicon wafer and annealed in a tube furnace under 7%/93% H_2/N_2. Figure 5 shows XRD patterns of the FePt@SiO_2 nanocrystals annealed at increasing temperature. First of all, the XRD peak widths do not narrow after annealing—until reaching temperatures of ~1000 °C—indicating that the primary particle size does not change and there is no sintering. Transmission electron microscopy images (Figures 5b and 5c) of FePt@SiO_2 nanocrystals annealed at 700 °C confirm that the FePt cores do not sinter. The silica-coated FePt nanocrystals transform to the $L1_0$ phase at about 650−700 °C. The unit cell transforms from cubic to tetragonal, and the (110) scattering peak that does not appear from the fcc material appears at $2\Theta \approx 34°$. The (111) diffraction peak also shifts to a slightly higher angle, confirming the fcc to $L1_0$ phase transition.

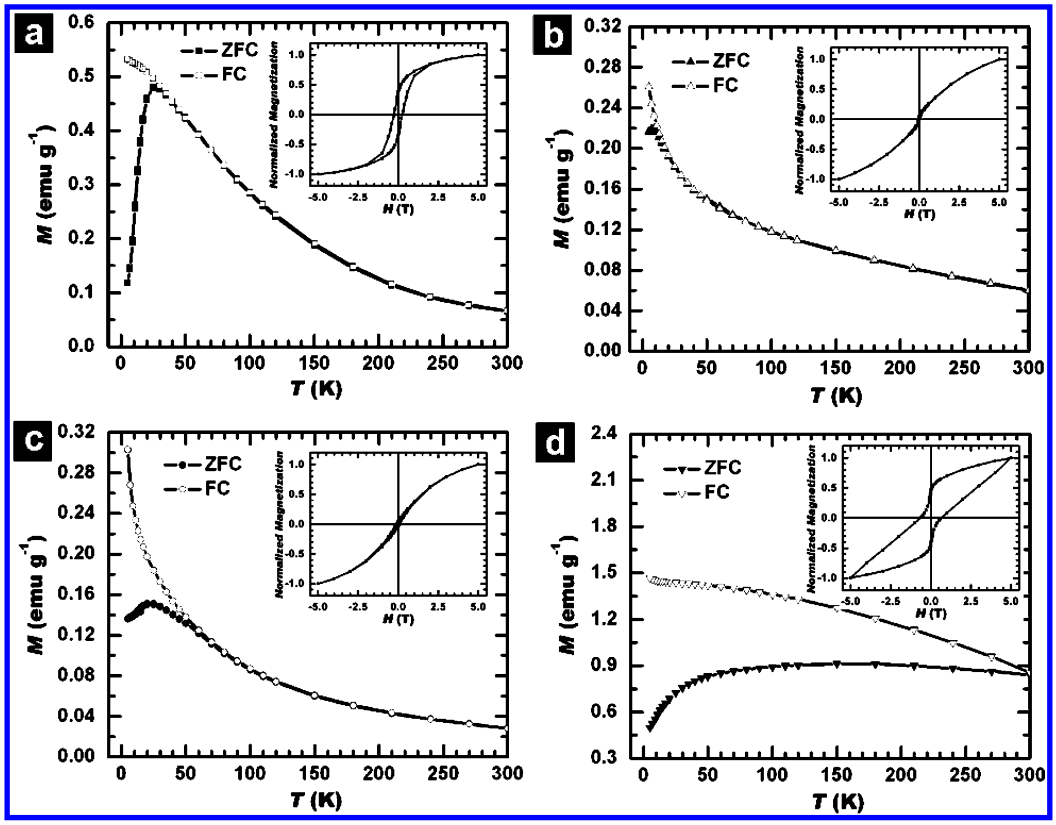

Figure 4. Zero-field-cooled (filled symbols) and field-cooled (empty symbols) magnetization scans of of FePt@SiO_2 particles: (a) as-made and annealed for 1 h at 700 °C in (b) air, (c) N_2, and (d) 7%/93% H_2/N_2. The particles annealed under H_2 exhibit a high blocking temperature, magnetic moment, and coercivity (~8000 Oe). The coercivity of the particles decreased when annealed under N_2 or air, although the saturation magnetization was higher after N_2 annealing than the as-made particles. Insets: Magnetization field scans acquired at 5 K.

The silica shell decomposes at ~1000 °C as shown in the TEM image in Figure 5d and revealed by the sharp intense diffraction peaks in Figure 5e. Additional peaks in the XRD pattern after annealing at 1000 °C correspond to cristobalite.[28] At 1000 °C, the SiO_2 shell crystallizes and no longer protects the FePt cores from coalescence.

The SiO_2 shell also affects the fcc to $L1_0$ phase transition. Unlike films of organic-monolayer-coated fcc FePt nanocrystals that transform to the $L1_0$ phase when annealed at ~550 °C under nitrogen,[28] the silica-coated FePt nanocrystals did not transform to the $L1_0$ phase when annealed under nitrogen or air—until reaching 1000 °C when the SiO_2 shell disintegrated. Figure 6 shows XRD patterns for FePt@SiO_2 nanocrystals annealed under nitrogen. The XRD pattern does not change until reaching 1000 °C. There is a clear difference between the XRD patterns of the FePt@SiO_2 nanocrystals annealed under hydrogen compared to those under nitrogen at 700 °C. Annealing under hydrogen was *required* for the fcc to $L1_0$ phase transition of FePt particles coated with silica.

Magnetic measurements confirmed that FePt@SiO_2 nanocrystals annealed under air or nitrogen at 700 °C did not undergo the fcc to $L1_0$ phase transformation, whereas those annealed under hydrogen were transformed. In fact, annealing under N_2 or air *decreased* the blocking temperature and the coercivity significantly (at 5 K H_c = 1000 Oe (N_2) and 200 Oe (air)) relative to the as-prepared sample (Figures 4B and 4C). The silica treatment in combination with high-temperature annealing appears to oxidize some of the FePt core to a softer magnetic material like iron oxide. We have found the silica coating chemistry to be quite oxidizing—NH_4OH is a strong oxidizing agent—and in fact, we have tried to coat semiconductor nanocrystals such as CdS and CdSe, but they are partially destroyed in the silica formation process. We have even found that $MnPt_3$ nanocrystals partially dissolve during the same silica coating procedure. FePt is much more robust than CdSe but could still be susceptible to surface oxidation. Annealing under a reducing environment such as hydrogen appears to reverse or prevent any oxidation that may occur as a result of the coating step.

However, we do not fully understand why hydrogen induces the fcc to $L1_0$ phase transition of the silica-coated nanocrystals, whereas nitrogen annealing does not. Perhaps the oxidative silica coating environment is the reason—oxidizing the nanocrystals to a small degree—however, XRD does not show evidence of oxidized species such as iron oxide in the FePt@SiO_2 nanocrystals annealed under air or nitrogen. It is certainly (although unlikely) possible that small amounts of residual FePt oxidation, undetectable by XRD or TEM, could be responsible for preventing the phase transition under air or nitrogen annealing. Another alternative explanation is that hydrogen itself facilitates the fcc to $L1_0$ phase transition, as others have found for FePt films.[29] Hydrogen atoms have been proposed to enter the FePt lattice and induce local strain to enhance Fe and Pt mobility and structural reordering,[30] although others studying similar FePt films have proposed that hydrogen simply reduces the presence of oxidized species.[31] H_2 can penetrate the SiO_2 shell in microseconds to reach the FePt core during annealing, as the diffusivity of H_2 in SiO_2 at 700 °C is 3.14×10^{-7} cm^2/s.[32]

Magnetic Properties of $L1_0$ FePt@SiO_2 Nanocrystals. Figure 4D shows FC and ZFC scans and field sweeps (at 5 K) on FePt@SiO_2 nanocrystals annealed under hydrogen at 700 °C. The coercivity at 5 K has increased relative to the as-made nanocrystals by a factor of 3 to 8 kOe. The saturation magnetization is large, and saturation is not reached, even at applied fields up to 5 T (50 kOe). The FC and ZFC scans indicate that the nanocrystals are superparamagnetic but that

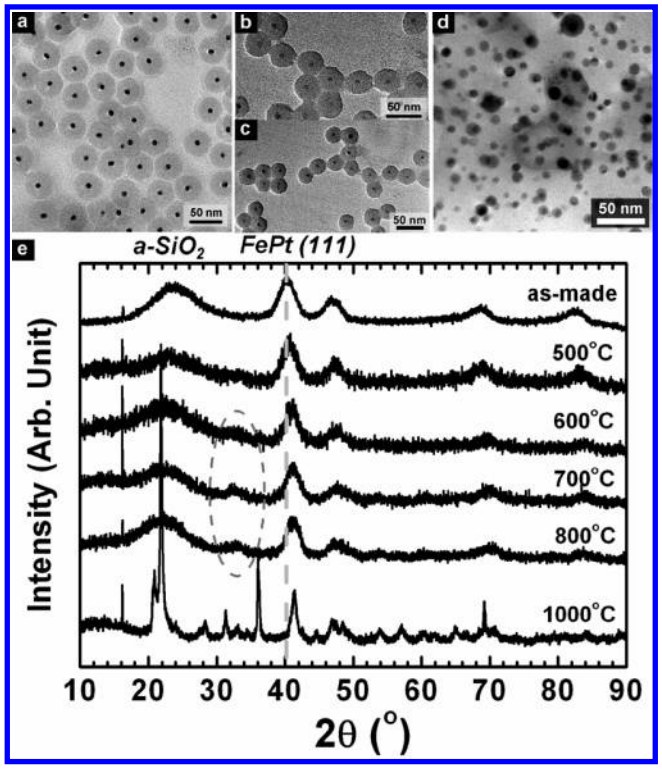

Figure 5. FePt@SiO_2 nanocrystals annealed under 7%/93% H_2/N_2 at different temperatures. Transmission electron microscopy images of FePt@SiO_2 particles: (a) as-made, (b−c) after annealing at 700 °C, and (d) after annealing at 1000 °C. The FePt cores do not coalesce during 700 °C annealing, but 1000 °C annealing leads to significant FePt particle aggregation and coalescence. (e) X-ray diffraction patterns of the annealed FePt@SiO_2 films annealed under H_2 at different temperatures. A phase transition from the random alloy fcc phase to the face-centered tetragonal (fct) $L1_0$ phase occurs when annealed at 600−700 °C; annealing at 1000 °C led to very sharp diffraction peaks as a result of structural collapse of the silica shell and FePt sintering as confirmed by TEM in part d. The labeled peaks indicate the evolution of the fct FePt phase. The (111) peak shift supports the occurrence of the phase transition at annealing temperatures between 600 and 700 °C.

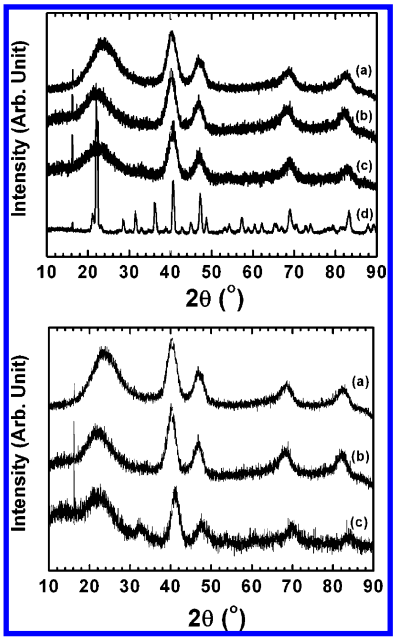

Figure 6. Top panel: X-ray diffraction patterns of FePt@SiO_2 particles annealed under N_2: (a) as-made and annealed at (b) 700 °C, (c) 800 °C, and (d) 1000 °C under N_2. Bottom panel: X-ray diffraction patterns of (a) as-made particles, (b) particles annealed at 700 °C under N_2, and (c) particles annealed at 700 °C under hydrogen.

the blocking temperature exceeds room temperature, which is confirmed by the observation of room temperature hysteresis in the field sweeps with relatively high coercivity ($H_c \approx 2300$ Oe).

The magnetization curves from the $L1_0$ FePt@SiO_2 nanocrystals exhibited "constricted" hysteresis loops near zero applied field (Figure 7b). The magnetization relaxes more abruptly than expected for a typical ferromagnet when the applied field direction is switched. A similar relaxation of the magnetization was observed recently from 4 nm diameter $L1_0$ FePt nanocrystals obtained from a high-temperature synthesis in the gas phase, which was attributed to a distribution in size or composition in the sample.[33] A magnetic sample that is a mixture of hard and soft magnetic material (i.e., large and small susceptibility, coercivity, and saturation magnetization) could give rise to these kind of magnetization curves, for example, if the hard magnetic $L1_0$ FePt cores contained some soft magnetic Fe or iron oxide associated with them. This is probably the case in ref 33, as the remanent field dropped to less than one-half of the saturation magnetization M_{sat} when the field was removed and the coercivity was very low, only ~0.05 T (500 Oe) at 4.3 K. In contrast, the coercivity of the $L1_0$ FePt@SiO_2 nanocrystals was typically between 0.5 and 1 T (5−10 kOe) at 5 K, and the remanence was always between $0.4M_{sat}$ and $0.5M_{sat}$. For a collection of nanocrystals with random crystallographic orientations, the applied field rotates the magnetic moments into the direction of the field at saturation, which may be away from the magnetic easy axis of the particle—this spin rotation away from the magnetic easy axis could be the reason for the relatively slow rise in magnetization at higher applied fields. When the field is removed, the magnetic moments in each particle relax to their magnetic easy axis, which is the [001] direction in $L1_0$ FePt. For a random (uniform) distribution of magnetocrystalline orientations, one expects a remanance of $(2/\pi)M_{sat}$ (assuming no thermal broadening of the spin orientation distribution), which is close to what is experimentally observed. Furthermore, impurities such as iron oxide and Fe did not show up in the XRD data.

The coercivity was observed to be a relatively strong function of silica shell thickness. As plotted in Figure 7c, the coercivity measured at 5 K varies from less than 0.1 T for shells less than 5 nm thick up to 1.1 T for 25-nm-thick shells. The remanence is approximately 0.45 times the saturation magnetization for all the samples, regardless of the shell thickness. These measurements seem to indicate that the shell thickness significantly affects the coercivity and most likely the constriction in the hysteresis curves is related to it. Certainly, the silica shell thickness determines the magnetic dipole coupling between nanocrystals, which for a bulk magnetic material determines the magnetic domain size and is responsible for ferromagnetic hysteresis. In these nanocrystals, the interparticle separation of several nanometers makes the dipole coupling *between* FePt domains relatively weak compared to the applied field energy and the magnetocrystalline anisotropy energy, yet the dipole coupling is relatively long range and varies as the inverse of the interparticle distance to the third power. Therefore, the dipole coupling between particles with 4 nm silica shells is about 2 orders of magnitude larger than the dipole coupling between particles with 25-nm-thick shells. Figure 7a shows a schematic of how the magnetic dipole coupling can influence the coercive field (the field strength required to reverse the magnetic spins). Magnetic dipole coupling between neighboring FePt nanocrystals can provide an additional demagnetization field, as dipole

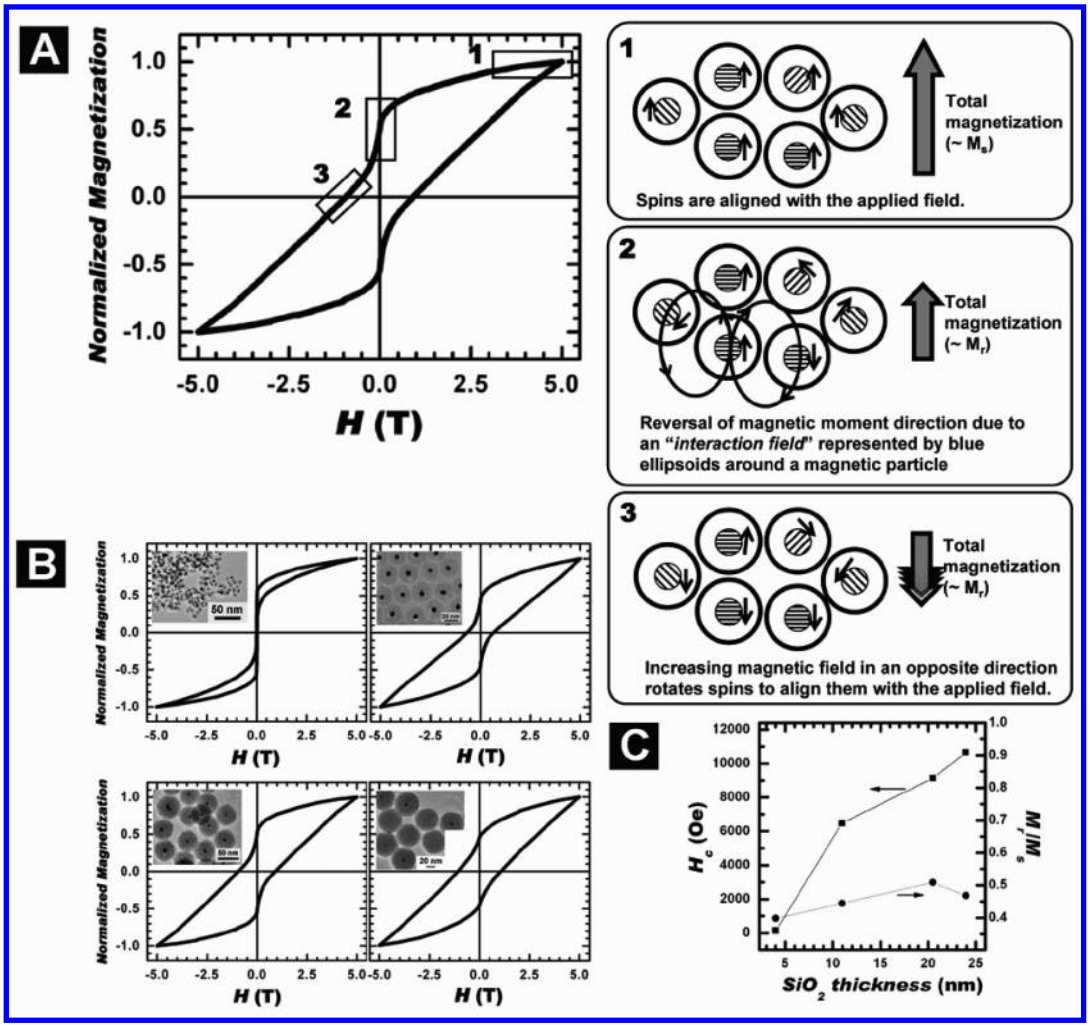

Figure 7. (A) Schematic illustration of magnetic dipole interactions in the FePt@SiO_2 particle film and their relationship to the $M-H$ curves. (B) $M-H$ curves (5 K) of FePt@SiO_2 nanocrystals (6 nm in diameter FePt core) with varying silica shell thicknesses measured after annealing at 700 °C in forming gas for 1 h. (C) Coercivity and normalized remanence measured as a function of SiO_2 thickness.

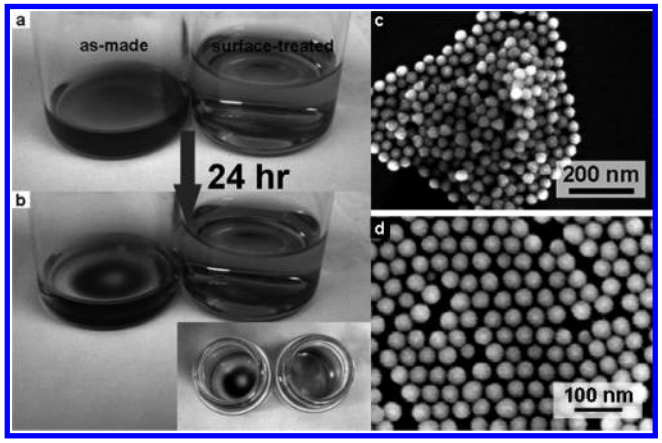

Figure 8. (a and b) Photographs of as-made and OTMOS-treated FePt@SiO_2 particles. Surface treatment makes the particles hydrophobic and prevents the flocculation that occurs with untreated particles. Scanning electron microscopy images of drop-cast particles (d) with and (c) without OTMOS treatment. The particles without surface functionalization tend to aggregate and do not crystallize into ordered structures.

coupling favors antiparallel alignment of neighboring spins. Recall that the FePt core diameter of all the samples shown in Figure 7 is the same, at 6 nm. It is very likely that magnetic dipole coupling between neighboring nanocrystals is reducing the coercivity and also leads to the constricted hysteresis loops.

Surface Treatment for Improved Dispersibility. The as-made FePt@SiO_2 particles disperse in ethanol/water solutions but exhibit a high degree of aggregation and sticking. For patterned deposition by spin-coating or drop-casting, better dispersions of FePt@SiO_2 particles are needed. Wang et al.[25] have developed a procedure for chemically treating silica colloids using OTMOS. The siloxane functional groups of OTMOS react with the silica surface when the particles are dispersed in chloroform for 24 h. The hydrophobic tails are then exposed at the surface to make the FePt@SiO_2 particles hydrophobic with good dispersibility in chlroform or hexane. Figure 8a shows dispersions of as-made FePt@SiO_2 particles in an alcohol solution and OTMOS surface-functionalized particles in organic solvents. Dispersions of the OTMOS-treated particles remained optically clear for months, while particles without surface treatment sedimented in 1 day. The SEM images in Figures 8c and 8d also show that the surface-treated particles form monolayers with better organization upon drop-casting than the particles with untreated surfaces.

Conclusions

Silica coatings were applied to colloidally grown oleic acid/oleylamine-capped FePt nanocrystals to prevent sintering during the high-temperature annealing required to convert the FePt core from the compositionally disordered, soft magnetic, fcc phase to the compositionally layered, tetragonal, hard magnetic, $L1_0$

phase. The silica coating prevents sintering at temperatures up to >850 °C. The silica shell could be modified with hydrophobic ligands (i.e., OTMOS) for good dispersibility in organic solvents. The magnetic measurements indicate that the coercivity is strongly dependent on the FePt separation set by the silica layer thickness, most likely due to differences in magnetic dipole coupling between FePt domains. The approach outlined here for silica shell growth could offer a general platform for obtaining better thermal stability of many different nanocrystals in thin films for high-temperature processing. However, the oxidizing environment in the silica shell growth process may be a limitation of the effectiveness of this particular shell growth chemistry. Other less basic catalysts other than NH_4OH might be useful for other materials systems.

Acknowledgment. We acknowledge the National Science Foundation (NSF; NIRT program, DMR-0210383; STC program, CTS-CHE-9876674), the Robert A. Welch Foundation, and the Advanced Prototype and Processing Center (DARPA HR00011-06-1-0005) for financial support. We thank U. M. Mirsaidov for assistance using the SQUID, V. M. Lynch and J. S. Swinnea for advice on XRD, and J. P. Zhou and J. Mendenhall for TEM assistance. J.M.P. thanks the NSF for financial support through the National Nanofabrication Infrastructure Network Research Experiences for Undergraduates Program at UT Austin (Program No. 44771-7476).

References and Notes

(1) Zeng, H.; Li, J.; Wang, Z. L.; Liu, J. P.; Sun, S. *Nano Lett.* **2004**, *4*, 187−190.

(2) Klemmer, T.; Hoydick, D.; Okumura, H.; Zhang, B.; Soffa, W. A. *Scr. Metall. Mater.* **1995**, *33*, 1793−1805.

(3) Weller, D.; Moser, A. *IEEE Trans. Magn.* **1999**, *35*, 4423−4439.

(4) Lambeth, D. N.; Velu, E. M. T.; Bellesis, G. H.; Lee, L. L.; Laughlin, D. E. *J. Appl. Phys.* **1996**, *79*, 4496.

(5) Sun, S. H.; Murray, C. B.; Weller, D.; Folks, L.; Moser, A. *Science* **2000,** *287*, 1989.

(6) For a recent review, see: Sun, S. *Adv. Mater.* **2006**, *18*, 393.

(7) Perez-Dieste, V.; Castellini, O. M.; Crain, J. N.; Eriksson, M. A.; Kirakosian, A.; Lin, J. L.; McChesney, J. L.; Himpsel, F. J.; Black, C. T.; Murray, C. B. *Appl. Phys. Lett.* **2003**, *83*, 5053.

(8) Konno, T. J.; Sinclair, R. *Acta Metall. Mater.* **1995**, *43*, 471.

(9) Yan, Q.; Kim, T.; Purkayastha, A.; Ganesan, P. G.; Shima, M.; Ramananth, G. *Adv. Mater.* **2005**, *17*, 2233−2237.

(10) Takahashi, Y. K.; Ohnuma, M.; Hono, K. *J. Magn. Magn. Mater.* **2002**, *246*, 259−265.

(11) Nguyen, H. L.; Howard, L. E. M.; Giblin, S. R.; Tanner, B. K.; Terry, I.; Hughes, A. K.; Ross, I. M.; Serres, A.; Bürckstümmer, H.; Evans, J. S. O. *J. Mater. Chem.* **2005**, *15*, 5136−5143.

(12) Reiss, B. D.; Mao, C.; Solis, D. J.; Ryan, K. S.; Thomson, T.; Belcher, A. M. *Nano Lett.* **2004**, *4*, 1127−1132.

(13) Mizuno, M.; Sasaki, Y.; Yu, A. C. C.; Inoue, M. *Langmuir* **2004**, *20*, 11305−11307.

(14) Chen, M.-P.; Kuroishi, K.; Kitamoto, Y. *IEEE Trans. Magn.* **2005**, *41*, 3376−3378.

(15) Elkins, K.; Li, D.; Poudyal, N.; Nandwana, V.; Jin, Z.; Chen, K.; Liu, J. P. *J. Phys. D: Appl. Phys.* **2005**, *38*, 2306−2309.

(16) Zeng, H.; Li, J.; Wang, Z. L.; Liu, J. P.; Sun, S. *Nano Lett.* **2004**, *4*, 187−190.

(17) Liu, C.; Wu, X. W.; Klemmer, T. J.; Shukla, N.; Weller, D.; Roy, A. G.; Tanase, M.; Laughlin, D. *Chem. Mater.* **2005**, *17*, 620.

(18) Chen, M.; Liu, J. P.; Sun, S. H. *J. Am. Chem. Soc.* **2004**, *126*, 8394.

(19) Tago, T.; Hatsuta, T.; Miyajima, K.; Kishida, M.; Tashiro, S.; Wakabayashi, K. *J. Am. Ceram. Soc.* **2002**, *85*, 2188.

(20) Santra, S.; Tapec, R.; Theodoropoulou, N.; Dobson, J.; Hebard, A.; Tan, W. *Langmuir* **2001**, *17*, 2900−2906.

(21) Yi, D. K.; Lee, S. S.; Papaefthymiou, G. C.; Ying, J. Y. *Chem. Mater.* **2006**, *18*, 614−619.

(22) Yi, D. K.; Selvan, S. T.; Lee, S. S.; Papaefthymiou, G. C.; Kundaliya, D.; Ying, J. Y. *J. Am. Chem. Soc.* **2005**, *127*, 4990−4991.

(23) Yamamoto, S.; Morimoto, Y.; Ono, T.; Takano, M. *Appl. Phys. Lett.* **2005,** *87*, 032503.

(24) Aslam, M.; Fu, L.; Li, S.; Dravid, V. P. *J. Colloid Interface Sci.* **2005**, *290*, 444−449.

(25) Wang, W.; Gu, B. H.; Liang, L. Y.; Hamilton, W. *J. Phys. Chem. B* **2003**, *107*, 3400.

(26) Osseo-Asare, K.; Arriagada, F. J. *J. Colloid Interface Sci.* **1999**, *218*, 68.

(27) Arriagada, F. J.; Osseo-Asare, K. *J. Colloid Interface Sci.* **1999**, *211*, 210.

(28) Yan, Q.; Kim, T.; Purkayastha, A.; Ganesan, P. G.; Shima, M.; Ramananth, G. *Adv. Mater.* **2005**, *17*, 2233−2237.

(29) Leistner, K.; Thomas, J.; Schlorb, H.; Weisheit, M.; Schultz, L.; Fahler, S. *Appl. Phys. Lett.* **2004**, *85*, 3498.

(30) Lai, C. H.; Wu, Y. C.; Chiang, C. C. *J. Appl. Phys.* **2005,** *97*, 10H305.

(31) Vedantam, T. S.; Liu, J. P.; Zeng, H.; Sun, S. *J. Appl. Phys.* **2003**, *93*, 7184.

(32) Doremus, R. H. *Diffusion of Reactive Molecules in Solids and Melts*; John Wiley & Sons: New York, 2002.

(33) Stappert, S.; Rellinghaus, B.; Acet, M.; Wassermann, E. F. *J. Cryst. Growth* **2003**, *252*, 440.